

Morphological Evolution of Distant Galaxies from Adaptive Optics Imaging

T.M. Glassman

glassman@astro.ucla.edu

J.E. Larkin ¹

larkin@astro.ucla.edu

and

D. Lafrenière

dlafre@astro.ucla.edu

Division of Astronomy, UCLA, 8371 Math-Sciences, Los Angeles, CA 90095

ABSTRACT

We report here on a sample of resolved, infrared images of galaxies at $z \sim 0.5$ taken with the 10-m Keck Telescope's Adaptive Optics (AO) system. We regularly achieve a spatial resolution of $0.05''$ and are thus able to resolve both the disk and bulge components. We have extracted morphological information for ten galaxies and compared their properties to those of a local sample. The selection effects of both samples were explicitly taken into account in order to derive the unbiased result that disks at $z \sim 0.5$ are ~ 0.6 mag arcsec⁻² brighter than, and about the same size as, local disks. The no-luminosity-evolution case is ruled out at 90% confidence. We also find, in a more qualitative analysis, that the bulges of these galaxies have undergone a smaller amount of surface brightness evolution and have also not changed significantly in size from $z \sim 0.5$ to today. This is the first time this type of morphological evolution has been measured in the infrared and it points to the unique power of AO in exploring galaxy evolution.

Subject headings: galaxies: evolution — galaxies: high-redshift — galaxies: spiral — galaxies: structure — techniques: high angular resolution

¹Alfred P. Sloan Research Fellow

1. Introduction

Observational constraints on the growth of galaxies and the role of star formation within them over time are finally within the reach of current data. Powerful new techniques, thanks to modern space-based and ground-based telescope facilities, have allowed researchers to make more precise measurements of galaxy properties. In this paper we focus on one aspect of this progress that is especially promising – resolved images of distant galaxies.

There has been a series of recent studies taking advantage of resolved data to measure the evolution of disk properties, especially B-band disk surface brightness to $z \sim 1$ from Hubble Space Telescope (HST) imaging. These studies have provided some constraints on the amount of evolution taking place, but there have been contradictory results, mostly due to disagreements about the impact of selection effects. Schade et al. (1996) and Roche et al. (1998) found B-band disk surface brightness evolution of ~ 1.6 mag to $z=0.73$ and ~ 0.95 mag to $z=0.9$, respectively, but neither focused on the impact of selection effects on their results. Lilly et al. (1998) also found a high level of surface brightness evolution (~ 0.8 mag to $z=0.67$), but calculated that as much as 0.3 mag of this could be due to selection effects. Vogt (1999) obtained rotation curves of galaxies to $z \sim 1$ and found relatively mild evolution in the Tully-Fischer relation ($\Delta M_B \lesssim 0.2$ mag), although their selection effects were very complicated. Simard et al. (1999) concluded that almost all of the disk surface brightness evolution they detected (~ 1.3 mag to $z=1$) is due to the selection effects. They also reanalyzed the Schade et al. (1996) and Roche et al. (1998) studies and found that selection effects could account for most of the evolution seen there as well. Both Vogt (1999) and Simard et al. (1999), however, do detect (even after accounting for selection effects) a population of galaxies at $z > 0.5$ that have higher surface brightness than the locus of nearby galaxies.

The progress derived from this resolved data has, moreover, been limited to observations of optical disk properties. To date the only resolved images of distant galaxies in the infrared (IR) have been those taken with NICMOS on HST. However these data mostly provided global colors and luminosities (e.g. Teplitz et al. 1998). The resolution of the camera ($\theta = 0.16''$) was insufficient to get reliable morphological information and profile fitting routines failed more than 50% of the time (Corbin et al. 2000). Observing in the IR reduces problems due to morphological K corrections that can arise with optical images which sample rest-frame ultraviolet (UV) light at high redshifts (e.g. Bunker et al. 2000). IR data more directly sample the mass distributions of distant galaxies since such images are less biased towards regions of high star formation.

Although a picture of the structure and kinematics of nearby bulges is beginning to emerge (Bureau 2002), resolved bulge observations have also been rare at high redshift. HST optical data does offer resolved images of bulges to $z \sim 1$, but most analysis of these

data has been confined to such things as bulge to disk ratios and bulge colors (e.g. Lilly et al. 1998; Ellis, Abraham, & Dickinson 2001).

In order to study resolved structures, including bulges, we have started a campaign to exploit high-resolution, IR images of distant galaxies from the 10-m Keck Telescope’s Adaptive Optics (AO) system. These data regularly have a resolution of $\sim 0.05''$ in the H band, equal to that of the HST optical data and three times higher than that of NICMOS. This resolution is sufficient to resolve bulges to arbitrary redshifts. The AO observations of the galaxies in our sample are described in §2 along with our methods of obtaining redshifts. In §3 we discuss the procedure used to extract galaxy morphological information from the AO images and in §4 we present the comparison of these data to a local sample, taking into account the selection effects for both samples. In §5 we discuss the implications of our result for galaxy evolution. Throughout this paper, we use $H_0=65 \text{ km s}^{-1} \text{ Mpc}^{-1}$, $\Omega_M=0.25$, and $\Omega_\Lambda=0.75$.

2. Observations

2.1. Sample Selection Using NIRC Imaging

Our strategy for finding target galaxies appropriate for AO observations involved searching near 26 bright stars using NIRC, a wide-field, non-AO, infrared camera on the Keck telescope (Matthews & Soifer 1994). From these fields, we selected a sample of ~ 150 galaxies that were chosen to fall within $30''$ of the bright stars and to have $K < 21.5$ mag in a $3''$ aperture. Many of the fields also contain faint, off-axis stars that are useful for calibrating the point spread function (PSF) of the AO observations. Objects found in these fields were named by the PPM designation of their guide star plus the offset (in arcseconds) from that star. Further details about these observations and the sample selection are presented by Larkin & Glassman (1999).

2.2. Adaptive Optics Observations and Data Reduction

From 1999 April to 2000 August, we observed 12 galaxies from this IR-selected sample with the Keck AO system (see Table 1). The observations through 1999 December were conducted with KCAM, the first-light camera on the Keck AO system, which has a field of view of $4.5''$ and a plate scale of $0.0175''$ per pixel. Observations in 2000 June and 2000 August were made with SCAM, the slit viewing camera on the NIRSPEC spectrograph (McLean et al. 1998), which has a field of view of $4.4''$ and a plate scale of $0.0172''$ per pixel.

in AO mode. Except for one, the galaxies were all observed in the H band ($1.65\ \mu\text{m}$) with additional observations for many of the galaxies in the J ($1.27\ \mu\text{m}$), K ($2.2\ \mu\text{m}$), and K' ($2.15\ \mu\text{m}$) bands. The 2000 August observations were the only ones made under non-photometric conditions.

The observations were dithered, moving the galaxy to each quadrant of the chip, so that the median of the object frames could be used as a sky. More elaborate dither patterns could not fit in the small field of view of the cameras used. A faint, off-axis star (with a guide-star offset matched to that of the galaxy) was observed as close in time to each galaxy observation as possible. In Table 1 the PSF star used to calibrate each galaxy observation is listed. In some cases, when no PSF was a perfect match, the galaxy observation was calibrated using two PSF stars that bracket the galaxy observing conditions (e.g. one is too close to the guide star and one is too far away). The off-axis PSF stars had full-width-half-maxima (FWHM) ranging from $0.05''$ to $0.15''$ and strehl ratios of $1 - 20\%$.

The data were reduced with standard IR procedures including sky subtraction, flat fielding, and dark subtraction. Super skies were generated from the science images by masking out the quadrant containing the galaxy or PSF star and taking the median of a stack of unaligned images. Bad pixels in the images were removed by replacing them with the average of their neighbors. In some cases, there were differences in the bias level between the four quadrants of the chip and/or the individual rows. These variations were removed by adjusting the clipped mean (calculated with the object masked out) of each quadrant/row to the average value for the entire image.

In order to combine dithered images of the same object, the separate frames had to be aligned. We found, through tests with the PSF images, that header or input offsets were only accurate to within a few pixels. Each object observed, including the galaxies, therefore had to be bright enough to centroid on in each individual 5-10 minute exposure. This is a strong limiting factor in the size and depth of the current sample. The aligned images were finally combined by averaging the frames together.

In the end, the 12 galaxies in the AO sample include all galaxies with $K < 18.5$ mag in a $3''$ aperture that were observable during the times we were at the telescope. This is bright enough to ensure accurate centroids and the sample is 100% complete to this photometric limit in the NIRC images.

2.3. LRIS Spectra and Redshift Determination

In order to obtain redshifts for the galaxies in our sample, we took spectra of eight of them with the Low Resolution Imaging Spectrometer (LRIS; Oke et al. 1995) on Keck in 1999 December, 2000 August, and 2001 July. The other four objects were not accessible during these times. Exposure times were 30-50 minutes and good continuum detections were made of seven of the galaxies.

Following the approach of Cohen et al. (1999), the redshifts were calculated manually from a visual determination of the wavelengths of spectral features. This technique is justified by the very low signal-to-noise (S/N) of the spectra, which would make it difficult for more automatic techniques to work. Also, the construction of template spectra for an automatic search would be difficult and not well justified for such a small number of objects.

For each spectrum analyzed, the wavelengths of all the spectral features were recorded, as well as the location of the 4000 Å break, if present. These features were then compared to the set of Hydrogen Balmer, Ca II, [OII], and CH lines. A redshift was determined from the best fit (lowest χ^2) of the wavelength of the observed features to the rest wavelength of the lines. When only a spectral break is present, the redshift was obtained from the location of the break only. One galaxy had a featureless spectrum, so no spectroscopic redshift was obtained for it.

We are also able to put limits on the redshifts of the six galaxies without spectroscopic redshifts because of the fact that the redshifts of galaxies with $K < 18.5$ mag are quite well constrained, as demonstrated by infrared-selected redshifts surveys (e.g. Cohen et al. 1996). Due to a conspiracy of low co-moving volume for low redshifts and the rapid fading of galaxies at high redshifts, our whole sample has an expected redshift distribution of $z = 0.6 \pm 0.3$, with a small percentage of galaxies expected at redshifts greater than $z = 1$. This agrees quite well with the average of our spectroscopic redshifts ($z = 0.55$). We used this information to assign a redshift probability distribution to the galaxies without spectroscopic redshifts. This full probability distribution was used in all of the analysis, but to simplify the plots, the galaxies without spectroscopic redshifts are shown at $z = 0.6$.

3. Extraction of Morphological Components

In order to compare our sample galaxies to local populations, we need to characterize their basic morphological attributes – i.e. separate them into disks and bulges and find the properties of each. The usual method of extracting this information is to create model disks and bulges and combine them to find the model that best matches the galaxy image. The

biggest difficulty in applying this method to our AO images is the low S/N per pixel; this limitation prevents us from doing a full 12-parameter, 2-dimensional analysis. In order to reduce the number of free parameters, in addition to increasing the S/N of the data, we decided to fit the models to the data in one-dimensional radial profiles. This approach has been used by many other authors and direct comparisons were made between this and other techniques in a few cases (e.g. de Jong 1996; hereafter DJ96).

We assumed that the bulges are round and that they can be characterized by exponential profiles, which eliminates three parameters (the position angle, inclination, and sersic index of the bulge). (Sersic profiles were tested for the bulges, but we found that these did not fit as well as exponentials.) We then estimated the position angles and inclinations of the disks by stretching them, while conserving flux, until they appeared, by eye, to be round (eliminating two more parameters). The central pixel of each galaxy was then determined by centroiding, followed by inspection of the radial profile to verify that it was smooth (eliminating a final pair of parameters). This left just five parameters to be determined by the formal χ^2 minimization routine: bulge peak surface brightness (μ_{oBulge}), bulge scale size (h_{Bulge}), disk peak surface brightness (μ_{oDisk}), disk scale size (h_{Disk}), and an additive sky background level. To further increase the S/N, as well as the strehl ratios, of the images in our sample, we focused on analyzing just the H-band images (except for PPM91714+18-17 which was only observed in K').

The errors on the galaxy profiles were derived by taking multiple azimuthal averages of the images while varying the position angle, inclination, and central pixel within reasonable ranges (typically $\pm 5^\circ$, $\pm 10\%$, and ± 1 pixel respectively). Four more profiles were created by taking the azimuthal average in four quadrants using the best fit position angle, inclination, and center. The standard deviation of the mean of all of these profiles was then taken as the error for each point. The final profiles were also binned into 6-7 radially averaged points (with the radial extent of the region we averaged over approximately proportional to the radius) in order to increase the S/N and to establish a smooth profile more representative of what we actually know about the galaxy and less subject to the effect of small fluctuations.

The small field of view, lack of true sky, and problems with the detectors for the AO images caused some additional difficulties. One issue was that the absolute level of the sky background in the AO images was a significant source of uncertainty. In order to put some constraint on this value for each image, we calculated the flux of each object in a $3''$ diameter aperture in both the pre-AO, NIRC image and the AO image. We then adjusted the background level of the AO image so that the magnitudes of the object in the two observations were the same. If the NIRC data was taken under non-photometric conditions or there was no NIRC data in the same band, the background level of the AO image was

estimated. However, this led to much higher errors for the AO photometry.

Another issue is that the AO galaxy profiles only had reasonable S/N out to $\sim 1'' - 2''$ radius. The result is that the characteristics of the outer portions of the galaxies' disks are poorly constrained by the AO images and the disk sizes are degenerate with the background offsets. In order to better characterize the outer regions of the disks, we fit models to both the AO images and the NIRC images of the same galaxies.

Model galaxies were created by making 2-dimensional, exponential disks and bulges, convolving each one with the PSF, adding together a disk and a bulge with a given flux ratio, and taking the azimuthal average of the resulting image. The best fitting model for each data set was found by minimizing χ^2 between the disk/bulge combinations and the data. For each set of model parameters, the χ^2 values for the two data sets were then added together to form a combined χ^2 . As expected, the NIRC images don't provide much of a constraint on the bulge characteristics (especially their sizes) since the bulges are unresolved in these images. However, they do help constrain the disk characteristics in ways that the AO images can't (see Figure 1). The final model for each galaxy was taken as the model with the lowest combined χ^2 value. One-sigma errors were found for each parameter by accepting models that produce a given range of χ^2 values ($\chi_{min}^2 + 7.04$ for six parameters).

3.1. Models and Tests

Various tests were conducted in order to confirm that our analysis methods were functioning correctly. We subtracted 2-D versions of the best-fit model from each galaxy image in order to examine the residual flux (see Figure 2). For the five galaxies for which we have tightly constrained fits, the residuals of the AO images contained less than 10% of the flux of the galaxy within a $3''$ aperture. The five with less well constrained fits still leave less than 30% residual flux in the AO images. These residuals are caused by a variety of effects. For the brighter galaxies with better constrained models, the primary cause is probably mismatches between the PSF in the galaxy image and the PSF used in the analysis. Another cause of residual flux is asymmetric structures or structures besides simple disks and bulges in the galaxies themselves. For the fainter galaxies with less well constrained models, large-scale noise fluctuations in the field are more likely to provide the dominant contribution to the residual flux. Several of the AO images of these galaxies have S/N as low as 3, which means that the 30% residuals could be simply due to noise in the images.

A small Monte-Carlo test was conducted to assess the effectiveness of the analysis routine in extracting the correct parameters. We randomly selected galaxy characteristics from a

sample of local galaxies (DJ96) and model galaxies were constructed using exponential disks and bulges with these parameters and random position angles (PAs) and inclinations for the disks. A small random sky level offset was included and the center of each galaxy was shifted randomly by a few pixels. Each model galaxy was then convolved with an AO and a NIRC PSF and residual images from our data were added to each to create appropriate noise and sky irregularities. Each model galaxy was then analyzed in the same way as our real galaxy images. Because so much of the analysis routine is done by hand, especially in finding the PA and inclination of the disk, only four model galaxies were fully analyzed. Still, this is enough to estimate the accuracy of the method. For the two models with small inclinations ($a/b < 1.25$), we found that the routine did a good job. The derived parameters for these two objects, including the inclinations, were all within 30% of their true values and 3/4 of them were within 15%. For the other two objects, which were closer to edge on ($a/b = 1.3$ and 2.3), the routine had less success. We underestimated the inclination for both of them (by $\sim 20\%$) and all the other derived parameters were therefore farther off from their input values (3/4 of them were more than 30% off). However, the errors appear to have a random nature; each parameter is underestimated and overestimated with about the same frequency, indicating no systematic shift in the derived parameters with respect to their real values. To use what we learned from these models about the accuracy of the analysis method, we calculated extra error terms that, when added in quadrature to the statistical $1\text{-}\sigma$ errors for each parameter, accounted for the difference between the input and calculated values of that parameter. This extra error term was derived for each of the four model galaxies and the mean of the four results was then added in quadrature to the $1\text{-}\sigma$ errors for the real galaxies.

We also wanted to assess the effect of PSF variation on our results and the repeatability of the derived morphological parameters. The galaxy PPM114182+6+27 (which was imaged during three different runs, under a variety of conditions) provided us with an opportunity to examine these issues. The conditions in 1999 September were highly variable with the strehl ratio of the off-axis PSF star changing from $\sim 9\%$ to $\sim 2\%$ over a period of 45 minutes. We used only the best-quality PSF and galaxy images in order to include the most information about the galaxy structure and to use the best matching PSF possible. This meant throwing out four of the seven images of the galaxy from this night. During the entire 2000 June run, the strehl was high ($\sim 10\%$) and stable and the conditions were photometric. We have two observations of the galaxy from this run, taken on two different nights. In 2000 August the observations were not photometric and the seeing conditions, while not offering a very high strehl, were stable. There are again two images from two different nights during this run. We analyzed all five of the images for this galaxy and found that the derived morphological parameters were consistent within the $2\text{-}\sigma$ error bars for all of the observations (see Figure 3) and within the $1\text{-}\sigma$ error bars for all but those in 1999 September. The June

observations, which were under the best conditions, had, as predicted, the smallest error bars and the best χ^2 values. As expected, the most discrepant point is the bulge size derived from the September image, when the conditions were most variable. This result gives us confidence that the morphology derivations are robust and that we have correctly modeled both systematic and random errors.

3.2. Results and Details of Individual Objects

Models that fit the data well were found for ten of the 12 galaxies, although five of the objects had large ranges of acceptable parameters. For the five best constrained galaxy fits, the average uncertainties on the four parameters were $\lesssim 30\%$. For the other five, less well constrained, fits the average uncertainties were $80\% - 150\%$ (except PPM50296-7-23 – see below). Although these uncertainties are large in a fractional sense, they actually occupy a small fraction of the available parameter space for normal galaxies. For two objects, no acceptable fit was found (see below). Table 2 lists the best fit for each successful case and Figure 4 shows the AO image of each galaxy along with the galaxy, PSF, and model profiles.

PPM91714+22-19 This galaxy has a good fit to the one H-band image and there is a small range of acceptable parameter space. The two galaxies we observed in this field are $5.1''$ apart and both are at $z=0.46$. It seems likely that they are interacting, although no significant distortion can be seen in the current images.

PPM102164+18-1 This galaxy has good fits to both H-band images. There is a small range of acceptable parameter space for the 2000 June image and a larger range for the 1999 December observation. The final model was obtained from a χ^2 weighted average of these two results. The galaxy is at a redshift of $z=0.55$.

PPM114182+6+27 The best images of this galaxy were from two separate observations in 2000 June (see above). The χ^2 weighted average of the results from these two observations was therefore used as the final model, providing a good fit with well-constrained parameters. The galaxy is at a redshift of $z=0.48$, but this was based only on the 4000\AA break, so it is less certain than the other redshifts ($\Delta z = \pm 0.05$).

This galaxy is unique in our sample in that the AO image shows a point source $0.6''$ south of the nucleus, with an apparent H-band magnitude of 22 (see Figure 4). The knot then has an absolute H-band magnitude of -20 and may be a very luminous star-forming region. Similar “super star clusters” are seen in local galaxies, but this would be among the most extreme examples and is about 2 mag brighter than the brightest

knot in the interacting galaxies NGC 6090 (Dinshaw et al. 1999). It is likely that the knot in PPM114182+6+27 is composed of many such regions or that it is a second galactic nucleus, indicating an ongoing merger. It could also simply be a companion galaxy seen in projection against the disk, although the projected separation is very small for this to be the case.

The probability of the knot being a faint Galactic star seen in projection against the disk is quite small. There is $\sim 1\%$ probability of a star of comparable magnitude being found within a $1''$ radius of this galaxy (Cohen 1994). This means that the chances of finding a star aligned with any galaxy in our sample is $\sim 12\%$.

PPM91088-21+18 There is a good, well-constrained fit to one of the H-band images of this galaxy (from 1999 September), but the fit to the other image (from 1999 December) is of lower quality (higher χ^2 and bigger errors) due to a much shorter exposure time. Therefore only the 1999 September result was used. This galaxy is at a redshift of $z=0.70$.

PPM101029+20-8 There is a good fit to the one H-band image of this galaxy, with a small range of acceptable parameter space. It was not observed with LRIS.

PPM50296-7-23 This is the only galaxy in our sample with a strong bar and we therefore could not analyze in the usual way. Instead, we took the azimuthal average in two 120° sections perpendicular to the bar. The disk was assumed to be face-on (i.e. no further correction for this was added) and the rest of the analysis proceeded in the normal way. The analysis resulted in a good fit with reasonable error bars on the parameters (average of 31%), however some of the light from the bar is certain to be contaminating the fit. For this reason the results are not considered to be of the best quality. This galaxy was not observed with LRIS.

PPM91714+18-17 There is a good fit to the only image of this galaxy, which is in the K' band. There is, however, a large range of acceptable parameter space – both disk parameters are only upper limits. The two galaxies we observed in this field are $5.1''$ apart and both are at $z=0.46$. It seems likely that they are interacting, although no significant distortion can be seen in the current images.

PPM106365-23+18 This galaxy has a good fit to the one H-band image, although there is a fairly large range of acceptable parameter space. The galaxy is at a redshift of $z=0.60$.

PPM127095-8+16 This galaxy has a good fit to the one H-band image, but there are rather poor constraints on the parameters and the AO and NIRC models disagree by a larger than average amount ($\gtrsim 60\%$). The galaxy was not observed with LRIS.

PPM106365+4+13 There is a good fit to the one H-band image of this galaxy. However, there is a very large range of acceptable parameter space. Both disk parameters and the bulge peak surface brightness have only upper limits and the bulge size is not constrained at all. It is the faintest galaxy in the sample at $K=18.4$ mag. Continuum light was detected in the LRIS spectrum of this source, but no features were seen that could be used to derive a redshift.

PPM102164+9+23 Because of the very short exposure time, the one AO image of this galaxy only had enough S/N to create a profile out to $\sim 0.5''$ radius, instead of the $1 - 2''$ radius typical for the AO images. Because of this, the AO profile could not be used to establish the photometry in place of the non-photometric NIRC image, nor was it useful in constraining the morphology of the galaxy. This galaxy was not included in our sample for the following evolutionary analysis. Since its exclusion is primarily based on the short exposure time, we do not consider this a significant bias to the sample. This galaxy was not detected in an LRIS spectrum.

PPM115546-4+6 This galaxy proved impossible to analyze successfully because a diffraction spike from the guide star passed very close to the galaxy in every image. This makes it impossible to get an uncontaminated profile of the galaxy, especially since the relative placement of galaxy and spike shifts with each image. At a separation of only $7''$, this galaxy is the closest to its guide star in the sample. It was not included in the following evolutionary analysis, but this should not bias the results. This galaxy was not observed with LRIS.

4. Comparing Local and Distant Galaxy Properties

The ten galaxies for which we have derived morphological parameters (all but PPM102164+9+23 and PPM115546-4+6) represent a flux limited sample with $K < 18.5$ mag within a $3''$ aperture. We next want to compare these properties to the same values for local galaxies. We accomplish this by creating a local comparison sample based on DJ96’s observations of 86 local disk galaxies. The morphological parameters of the galaxies in this sample were measured across a wide range of wavelengths using several different techniques – including fitting exponential disks and bulges to 1-D profiles in the H and K bands. DJ96 also provided an analysis of the selection effects present in their sample and an estimate of the volume-limited, bivariate, K-band distribution function of local disk properties. The main difficulty in using the DJ96 sample is that it contains primarily Sb- to Sd-type galaxies. Our galaxies are not inconsistent with this range of Hubble types, but we cannot properly determine type and there may be early-type disk galaxies in our sample. As discussed in §5, we don’t believe

this has a significant effect on IR surface brightness.

Starting with the volume-limited distribution function provided by DJ96, we used Monte-Carlo techniques to create a large, random sample of galaxy disks. We then found the highest redshift for each galaxy that would allow it to be included in our data set (based on our selection criterion of $K < 18.5$ mag within a $3''$ aperture and taking into account the K-band K correction versus redshift; Mannucci et al. 2001) and calculated a probability for each galaxy that is proportional to the comoving volume out to this limiting redshift. This probability was used to create a smaller, selected sample which represents our data set if there is no evolution present. The rest-frame properties of these objects were then adjusted from K-band to H-band surface brightness using $H-K=0.24$ (Mannucci et al. 2001) in order to directly compare them to our H-band AO data. Figure 5 shows the disk properties of this Monte-Carlo, no-evolution, H-band sample compared to these same properties for our sample.

The figure suggests that there is evolution between the two samples, in the sense that a larger fraction of our population than of the Monte-Carlo sample is at high surface brightness (< 16.5 mag arcsec $^{-1}$). To formally compare the two and quantify this evolution, we used the 2-D Komolgorov-Smirnov test (K-S; Press et al. 1996) which measures the probability of two samples being drawn from the same parent population. We used Monte-Carlo techniques, taking into account the error bars on our data, to derive a probability distribution function for the K-S value that is specific to our data set. Based on this distribution function and the K-S value between our measured data and the no-evolution sample, we found that there is $< 10\%$ chance of getting our data if there is no evolution in the galaxy population.

To test what type of evolution is most consistent with the two measured populations, we shifted the size and peak surface brightness of all the galaxies in the Monte-Carlo sample created from DJ96’s distribution function. We then reapplied our selection effects to create several random samples with varying amounts of evolution and used the K-S test to compare each one to our data. This is a very simple model of galaxy evolution in that all galaxies change by the same amount, however it does provide a way to measure the shift in the average properties between the two populations. As Figure 6 shows, the best match occurs if galaxy disks at moderate redshifts were ~ 0.6 mag arcsec $^{-2}$ brighter than and about the same size as local disks. This amount of disk evolution is consistent with our data at the 75% level. The no-evolution case is in the middle-left edge of the plot and is strongly ruled out. There is some degeneracy seen in this plot due to the weak correlation of size with surface brightness in the galaxy population. The result is that we are more sensitive to evolution that changes the average luminosity of the galaxies than to evolution along lines of constant luminosity. If we accept all models that match our data with at least a 65% probability,

we conclude that the disks of galaxies to $z \sim 0.5$ have evolved by $\sim 0.6^{+0.3}_{-0.1}$ mag arcsec $^{-2}$ in surface brightness and by a factor of 0.8 to 1.05 in size.

We now turn to a key advantage of these AO images over previous galaxy surveys – the fact that all of the high-redshift bulges in our sample are resolved. However, comparing these bulges to those nearby is not straightforward. Since the disks are the primary drivers of the selection effects that define both distant and local samples, removing these effects from the bulge statistics is difficult. As a first attempt, we chose actual galaxies out of DJ96’s sample whose H-band disk properties are consistent with galaxies in the selected, no-evolution disk sample. We then compared the bulge properties of these galaxies to the bulge properties of our sample. In Figure 7, both disk and bulge properties of this sub-sample of DJ’s data and our objects are plotted. The amount of bulge surface-brightness evolution appears to be slightly less than that measured for the disks. There are some bulges whose surface brightness is higher than that of most local galaxies, but this is a smaller fraction than for the disks. The sizes of the bulges are within $\sim 5\%$ of local sizes and therefore also show little evolution. It is important to remember, however, that this might be a biased comparison. In order to quantify these conclusions and put limits on the amount of bulge evolution consistent with our data, we need to do a full, four-parameter analysis of all the selection effects, which would require a larger sample size.

5. Implications for Galaxy Evolution

We have measured 0.6 mag arcsec $^{-2}$ of surface brightness evolution through the use of IR, AO observations of galaxies at $z \sim 0.5$. This result is consistent with previous B-band results, mostly from HST studies (e.g. Schade et al. 1996; Roche et al. 1998; Lilly et al. 1998; Vogt 1999; Simard et al. 1999) although there has been controversy over whether the evolution seen in these studies is real or due to selection effects. We believe that we understand our selection effects and that any influence they had on the samples were removed. By matching the selection effects of the two samples and creating a Monte-Carlo, no-evolution sample we can directly measure what the local population looks like when subjected to our selection criterion, including removing any low-surface brightness galaxies we would have missed. Even with this taken into account, there is a shift in the average surface brightness of the disk population. We therefore believe that this evolution is real.

One caveat to this conclusion is that DJ96’s sample included only late-type spiral galaxies. Since our sample was not selected according to Hubble type, we presumably include disk galaxies of all types. This difference could lead to a bias in the comparison if the disk surface brightness of the S0 and Sa galaxies, that we include but DJ96 don’t, is much higher than

for the later types. Local samples, however, show that this is not the case; there is very little change in the K-band, mean disk surface brightness between early- and late-type spirals (Graham 2001).

Our results are also generally consistent with the models constructed by Bouwens & Silk (2002). They explore two types of models and compare their predictions to the previous, B-band observations of disk surface brightness evolution. The hierarchical models scale the galaxy disk properties with the properties of the dark matter halos in which they form. The infall models concentrate on the conversion of gas into stars, as constrained by observations of the Milky Way and other nearby galaxies. The star formation rate is taken to fall off with galactic radius and the luminosity of the galaxy at each radius is calculated versus time from spectral synthesis codes. Their models predict ~ 1.5 mag of B-band surface brightness evolution to $z \sim 1$, which they find is consistent with the level of evolution observed. However, the models all give about the same predictions for the surface brightness and size evolution, so it was not possible for them to distinguish between the various models.

The fact that our measurement of disk surface-brightness evolution was made in the IR which samples rest-frame optical light at high redshift, rather than in the optical which samples rest-frame UV at high redshift, significantly reduces the uncertainties in both the photometric and morphological K corrections. This data is less subject to the effects of a recent burst of star formation and the measured shift more likely represents a change in the underlying stellar population. Although Bouwens & Silk (2002) don't make any predictions of galaxy evolution when observed in the IR, the level of evolution we see is generally consistent with the previous data and with these models. Pozzetti, Bruzual, & Zamorani (1996) constructed a simpler, pure luminosity evolution model from which they do make predictions in the IR. Their K-band predictions, for an $\Omega=0$ universe, range from 0.4 mag of brightening to $z=0.5$ for a single-burst population to 0.3 mag of fading to $z=0.5$ for a constant star-formation model. The level of brightening we observe would clearly require some amount of bursting star formation under this model. Recent stellar-population models, specifically designed for intermediate-age populations and accounting in a self-consistent manner for AGB stars, have suggested that these stars could lead to 0.3-0.5 mag of brightening in the K band for populations 0.5-5 Gyr old, relative to models where these stars are neglected (Mouhcine & Lançon 2002a,b). This could reconcile the Pozzetti et al. (1996) models with our observations.

Even if the average properties of the high-redshift sample can't constrain specific models of galaxy formation, it is clear that there is a population of galaxies at high redshift that have higher surface brightness than almost all galaxies seen locally. From our Monte-Carlo model, based on local galaxy properties, we would expect less than 20% of the disks in our sample

to have a surface brightness above $16.5 \text{ mag arcsec}^{-2}$, whereas we actually observe half of our objects above this limit. There is no reason why these bright disks wouldn't be detected in the local sample since they have normal scale lengths and high surface brightness. This observation matches that made by both Vogt (1999) and Simard et al. (1999), that there is a population of high redshift galaxies with surface brightness higher than the locus of local galaxies. The most likely explanation for these objects is that they have a younger stellar population than local galaxies and therefore their surface brightness will fade with redshift and they will become the normal galaxies seen today. Simard et al. (1999) suggest two other possibilities to explain these objects: they are a type of galaxy at high redshift that doesn't exist today or they are members of a rare population that was therefore missed in the local sample (e.g. starburst HII galaxies). While we can't firmly rule these out until we have better statistics, the passive evolution model is definitely the simplest.

The lack of any observed, morphological evolution in the bulge population is generally consistent with the simple picture that bulges contain a uniformly old stellar population with little growth after an initial burst. This is the first time the morphologies of bulges at high redshift have been investigated, so there are no previous observations or models to compare our results to. Moreover, since the bulge evolutionary measurements we made were only qualitative, we can't make any strong statements about their effect on the larger picture of bulge evolution.

The data presented here are just the first part of a larger sample of resolved, IR observations of distant galaxies. Future samples will greatly increase the number of objects included and the quality of the data. These observations should provide stronger constraints on the amount of galaxy evolution taking place. Future models will hopefully be more detailed and make specific predictions tailored to these measurements. This combination should be a powerful tool in determining how galaxies form and evolve.

We thank the Keck staff for creating the Keck AO facilities, without which the observations reported here could not have been performed. We thank Dr. Ian McLean and the NIRSPEC team for a great instrument and early collaborations on this research. We also thank Dr. Robert Cousins for useful discussions.

This work has been supported in part or full by the National Science Foundation Science and Technology Center for Adaptive Optics, managed by the University of California at Santa Cruz under cooperative agreement No. AST-9876783. Dr. James Larkin would also like to acknowledge the Alfred P. Sloan foundation for their support through the faculty fellowship program.

Data presented herein were obtained at the W.M. Keck Observatory, which is operated

as a scientific partnership among the California Institute of Technology, the University of California, and the National Aeronautics and Space Administration. The Observatory was made possible by the generous financial support of the W.M. Keck Foundation. The authors wish to extend special thanks to those of Hawaiian ancestry on whose sacred mountain we are privileged to be guests. Without their generous hospitality, none of the observations presented herein would have been possible.

REFERENCES

- Bouwens, R. & Silk, J. 2002, *ApJ*, 568, 522
- Bunker, A., Spinrad, H., Stern, D., Thompson, R., Moustakas, L., Davis, M., & Dey, A. 2000, preprint (astro-ph-0004348)
- Bureau, M. 2002, preprint (astro-ph-0203471)
- Cohen, J. G., Hogg, D. W., Pahre, M. A., Blandford, R., Shopbell, P. L., & Richberg, K. 1999, *ApJS*, 120, 171
- Cohen, J., Hogg, D. W., Pahre, M. A., & Blandford, R. 1996, *ApJ*, 462, L9
- Cohen, M. 1994, *AJ*, 107, 582
- Corbin, M. R., O’Neil, E., Thompson, R. I., Rieke, M. J., & Schneider, G. 2000, *AJ*, 120, 1209
- de Jong, R. S. 1996, *A&A*, 313, 45 (DJ96)
- Dinshaw, N., Evans, A. S., Epps, H., Scoville, N. Z., & Rieke, M. 1999, *ApJ*, 525, 702
- Ellis, R. S., Abraham, R. G., & Dickinson, M. 2001, *ApJ*, 551, 111
- Graham, A. W. 2001, *MNRAS*, 326, 543
- Larkin, J. E., & Glassman, T. M. 1999, *PASP*, 111, 1410
- Lilly, S., et al. 1998, *ApJ*, 500, 75
- Mannucci, F., Basile, F., Poggianti, B. M., Cimatti, A., Daddi, E., Pozzetti, L., & Vanzi, L. 2001, *MNRAS*, 326, 745
- Matthews, K., & Soifer, B. T. 1994, *Exp. Astron.*, 3, 65
- McLean, I. S., et al. 1998, *Proc. SPIE*, 3354, 566
- Mouhcine, M. & Lançon, A. 2002, *A&A*, in press
- Mouhcine, M. & Lançon, A. 2002, *A&A*, in preparation
- Oke, J. B., et al. 1995, *PASP*, 107, 395
- Pozzetti, L., Bruzual, G., & Zamorani, G. 1996, *MNRAS*, 281, 953

- Press, W. H., Teukolsky, S. A., Vetterling, W. T., & Flannery, B. P. 1996, Numerical Recipes in Fortran 77: The Art of Scientific Computing, Vol. 1 (2d ed.; Cambridge: Cambridge University Press)
- Roche, N., Ratnatunga, K., Griffiths, R. E., Im, M., & Naim, A. 1998, MNRAS, 293, 157
- Schade, D., Lilly, S., Le Fevre, O., Hammer, F., & Crampton, D. 1996, ApJ, 464, 79
- Simard, L., et al. 1999, ApJ, 519, 563
- Teplitz, H. I., Gardner, J. P., Malumuth, E. M., & Heap, S. R. 1998, ApJ, 507, L17
- Vogt, N. P. 1999, in ASP Conf. Ser. 193, The Hy Redshift Universe, ed. A. J. Bunker, & W. J. M. van Breugel (San Francisco: ASP), 145

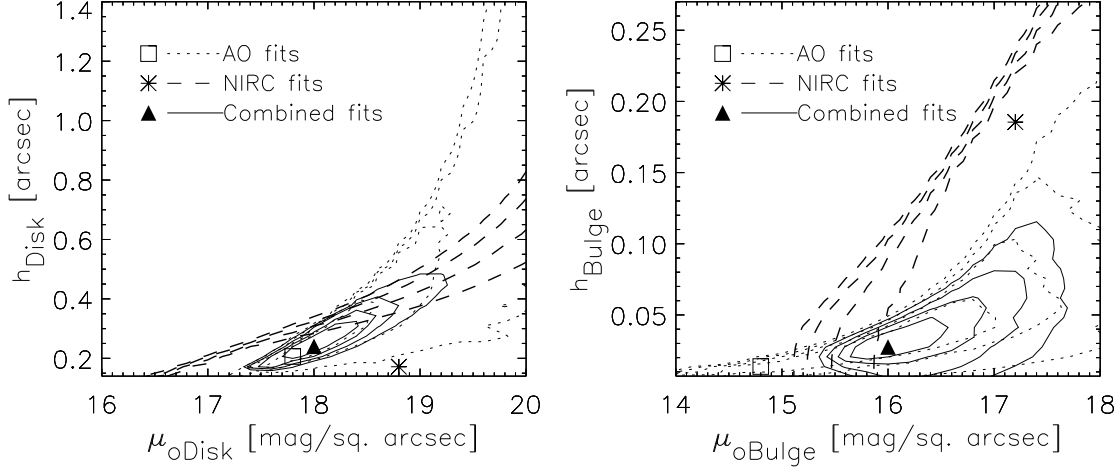


Fig. 1.— A representative example of the results of the χ^2 fitting routine (for the galaxy PPM101029+20-8) is shown. Contours of χ^2 at 1, 2, 3, and 4- σ above the minimum are plotted with respect to the four tested parameters (disk size and surface brightness on the left, bulge size and surface brightness on the right). The three sets of contours are for fits to just the galaxy profile from the AO image, fits to just the galaxy profile from the NIRC image, and the sum of the χ^2 values for these two. The points mark the best fitting model for each of the three cases. As is fairly typical, the addition of the NIRC information restricts the result to models with smaller disk sizes than does the AO data alone, but it has less of an effect on the bulge parameters. This is consistent with the partial degeneracy between the disk size and the sky background seen with the AO data, due to the small field of view of these images. Although each data set by itself can lead to degeneracies in the model parameters, the two data sets are complementary and therefore constrain the parameters quite tightly when used together.

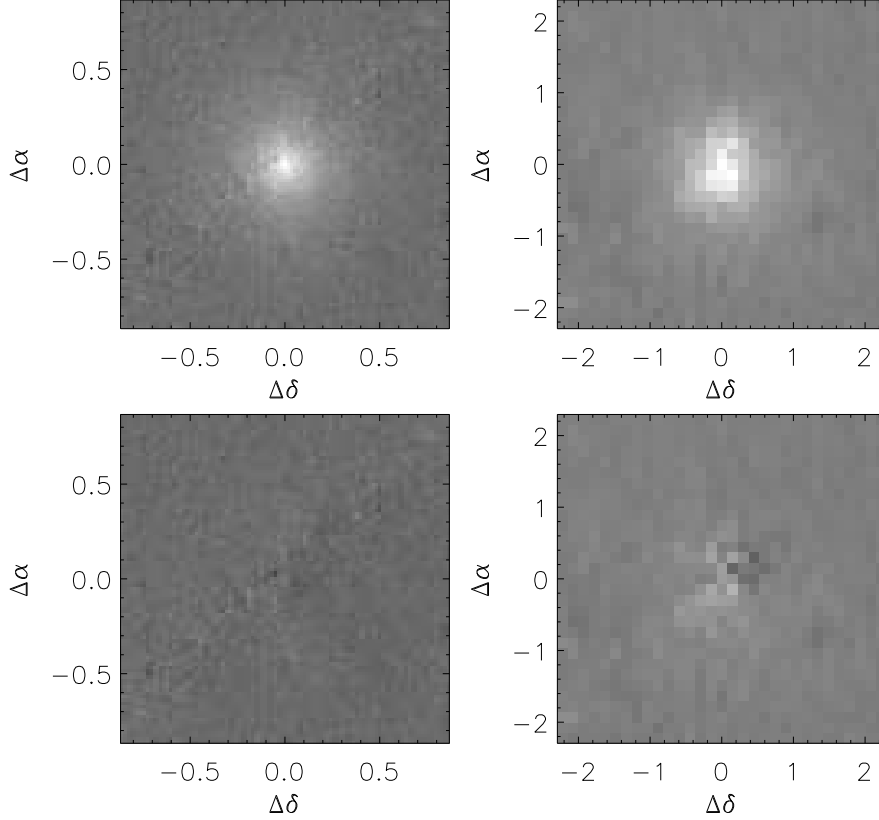


Fig. 2.— Shown above are the AO (top left) and NIRC (top right) images of the same galaxy (PPM102164+18-1), along with the residuals (bottom) obtained when the best combined-fit model is subtracted from each. The greyscales used to make these images are the same for the original and the residual image in each pair. It can be seen that there is relatively little residual flux, although the NIRC residual is slightly worse than the AO residual in this case: there is 20% residual flux in the NIRC image, as opposed to 7% residual flux in the AO image. The residuals in this case are representative of the rest of our sample.

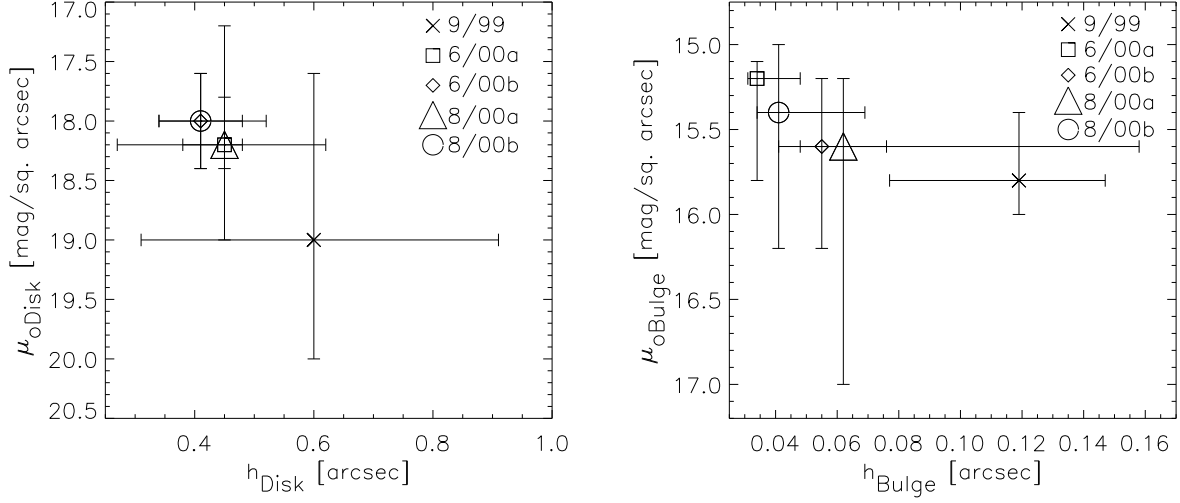


Fig. 3.— Shown here is a comparison of morphological parameters derived from five separate AO images of the galaxy PPM114182+6+27. On the left hand side are the disk parameters (size and surface brightness) and on the right are the same parameters for the bulge. The five disk models are consistent within the $2\text{-}\sigma$ error bars, as shown in the plot. For the bulge, the only discrepant point is from 1999 September, as expected.

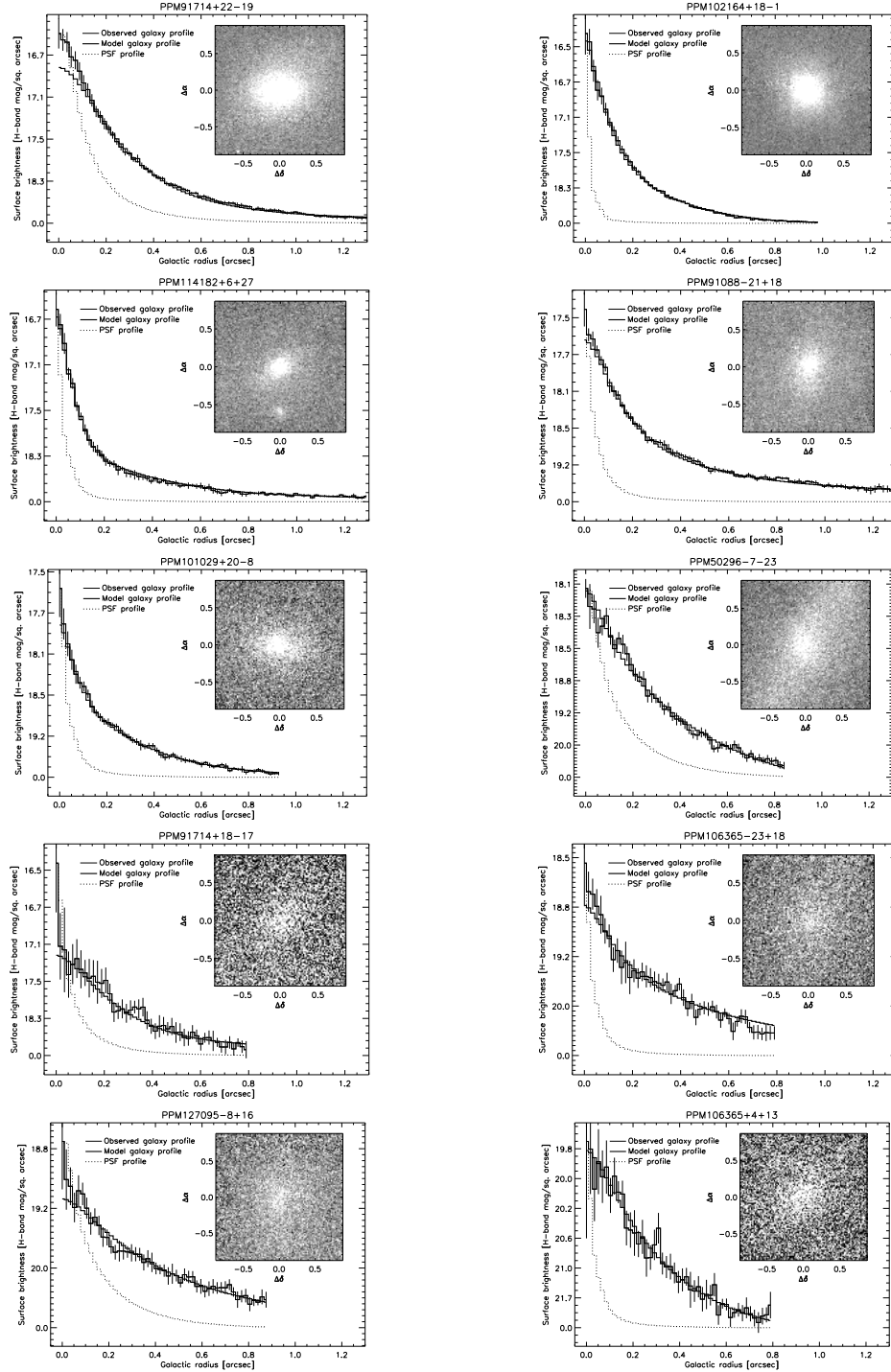


Fig. 4.— The AO image of each galaxy that had a successful morphological fit is shown here, along with profiles of the AO image of the galaxy, the AO PSF, and the model that best fits the combination of AO and NIRC data. The large variety in the data quality, the PSF shape, and the model success can be seen here. Note the off-axis point source to the south of the galaxy PPM114182+6+27 and the strong bar in PPM50296-7-23.

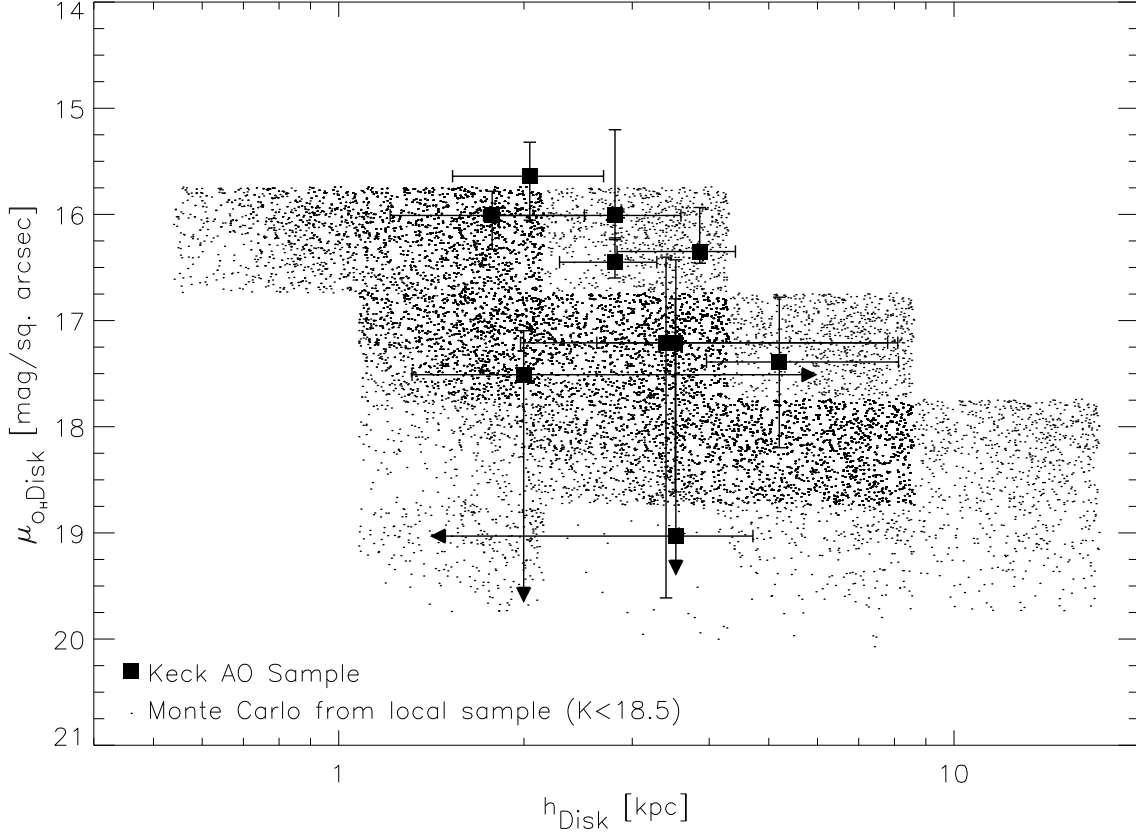


Fig. 5.— Plotted here (small dots) are the H-band disk properties expected for our galaxy sample if there is no evolution in the population, based on the properties of a local galaxy survey (DJ96) and the selection effects of both samples. The boxes with error bars show the same properties for the galaxies in our sample. The galaxies in our sample without known redshifts are shown here as if they were at $z=0.6$ but the full allowed range of redshifts was taken into account in the quantitative analysis. The edges in the local sample distribution come from the discrete method used by DJ96 to model their volume correction.

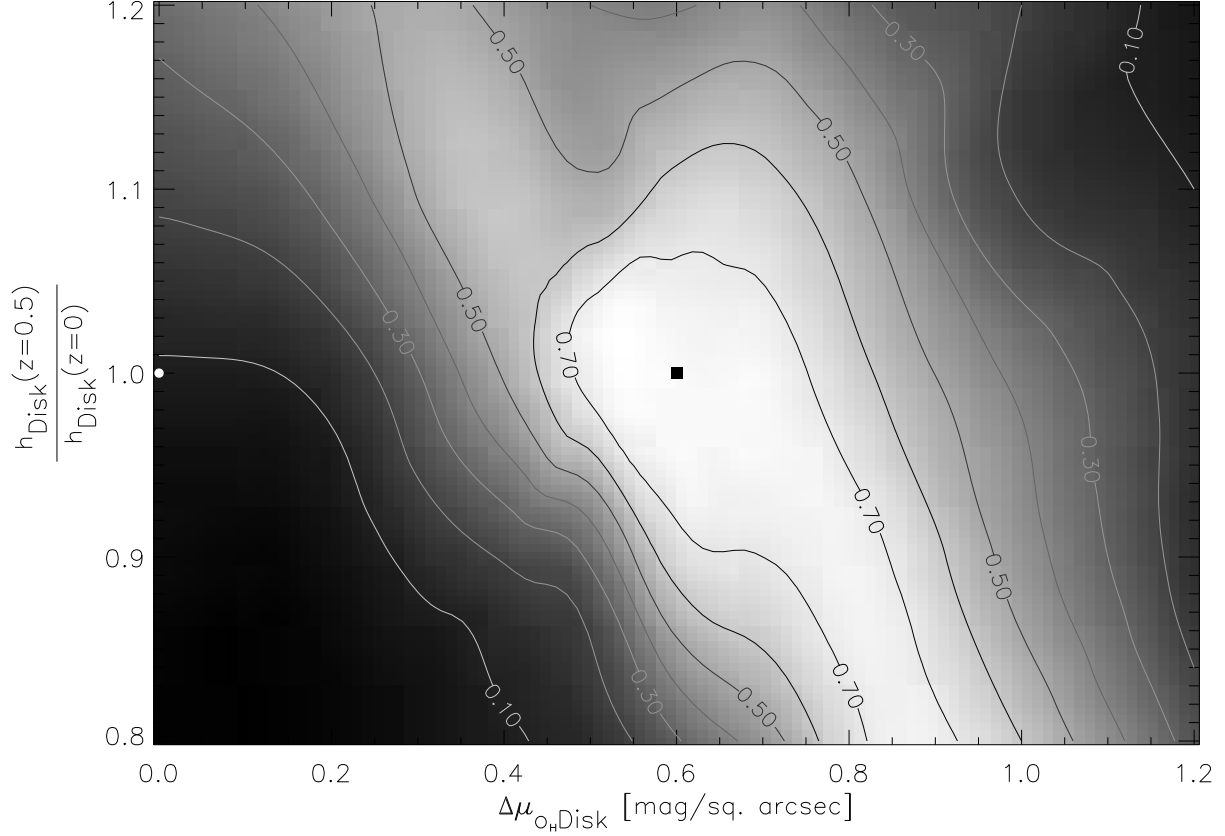


Fig. 6.— Contours and greyscale of the probability of getting our AO data given the varying amounts of disk evolution are shown. The axes are magnitudes arcsec^{-2} of surface brightness evolution and fraction of size evolution. The best agreement between the two samples occurs if the disks in the distant sample are $0.6 \text{ mag arcsec}^{-2}$ brighter than and about the same size as local disks (marked in the plot by a black square). Note that the no-evolution case is at the middle-left side of the plot (white circle) and is ruled out at the 90% confidence level.

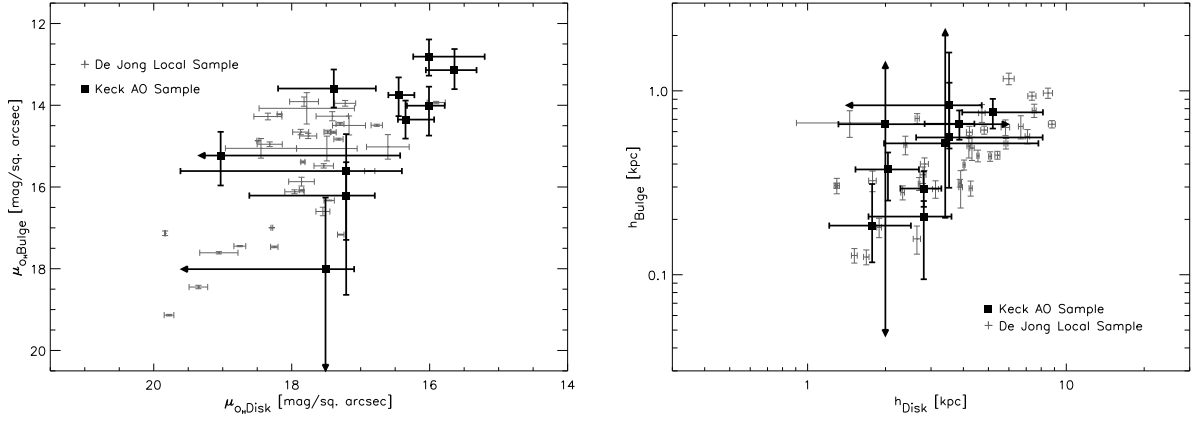


Fig. 7.— The surface brightness (left) and size (right) of the disks and bulges of our galaxies (bold) and a select sub-sample of DJ96’s galaxies (grey) are shown. The bulges appear to undergo slightly less evolution in surface brightness than the disks and there is no apparent change in the sizes of either component.

Table 1. AO Observations

Object ^a	K ^b	Date ^c	Band ^c	Time (min) ^c	PSF star ^d	FWHM (″) ^e	Strehl (%) ^e
PPM50296-7-23	16.7	1999 Dec	H	35	PPM127095-18+3	0.13	1.2
PPM91714+22-19	17.0	1999 Sep	H	35	PPM91714+9-19	0.16	1.3
PPM91714+22-19	17.0	2000 Aug	K′	80	PPM91714+9-19	0.08	5.6
PPM102164+18-1	17.0	1999 Dec	H	40	PPM127095-18+3	0.13	1.2
PPM102164+18-1	17.0	1999 Dec	J	30	PPM127095-18+3	0.45	0.2
PPM102164+18-1	17.0	2000 Jun	H	48	PPM102164-4+4/PPM106365-17+10	0.04/0.06	34.2/7.8
PPM102164+18-1	17.0	2000 Jun	K′	20	PPM106365-17+10	0.07	8.1
PPM102164+18-1	17.0	2000 Jun	J	40	PPM106365-17+10	0.14	0.9
PPM114182+6+27	17.1	1999 Sep	H	35	PPM114182+14+20	0.05	5.5
PPM114182+6+27	17.1	2000 Jun	H	48	PPM114182+14+20	0.05/0.06	10.3/7.0
PPM114182+6+27	17.1	2000 Jun	K	20	PPM114182+14+20	0.06	19.4
PPM114182+6+27	17.1	2000 Jun	J	20	PPM114182+14+20	0.09	3.3
PPM114182+6+27	17.1	2000 Aug	H	55	PPM114182+14+20	0.14/0.11	1.8/2.5
PPM91088-21+18	17.6	1999 Sep	H	45	PPM91088-23+12	0.07	5.4
PPM91088-21+18	17.6	1999 Dec	H	15	PPM91088-23+12	0.19	0.6
PPM91714+18-17	17.6	2000 Aug	K′	50	PPM91714+9-19	0.08	5.6
PPM106365-23+18	17.7	2000 Jun	H	20	PPM106365-17+10	0.06	7.8
PPM106365-23+18	17.7	2000 Aug	K′	50	PPM106365-17+10	0.07	9.0
PPM101029+20-8	18.1	2000 Jun	H	30	PPM101029+4-5/PPM106365-17+10	0.04/0.06	17.3/7.8
PPM101029+20-8	18.1	2000 Jun	K′	40	PPM106365-17+10	0.07	8.1
PPM102164+9+23	18.2	2000 Jun	H	12	PPM102164-4+4	0.04	34.2
PPM127095-8+16	18.2	1999 Dec	H	20	PPM127095-18+3	0.13	1.2
PPM127095-8+16	18.2	1999 Dec	J	20	PPM127095-18+3	0.45	0.2
PPM127095-8+16	18.2	1999 Apr	H	30	PPM127095-18+3	0.05	5.4
PPM115546-4+6	18.3	1999 Sep	H	30	PPM115546	0.07	6.5
PPM115546-4+6	18.3	2000 Jun	H	35	PPM115546/PPM106365+7+6	0.05/0.05	17.3/18.5
PPM115546-4+6	18.3	2000 Aug	K′	40	PPM115546	0.06	32.0
PPM106365+4+13	18.4	2000 Jun	H	60	PPM106365-17+10	0.06	7.8
PPM106365+4+13	18.4	2000 Aug	K′	40	PPM106365-17+10	0.07	9.0

^aThe galaxies and PSF stars are named by the PPM designation of their guide star plus the offset (in arcseconds) from that star.

^bK-band magnitude of the galaxy from the NIRC images.

^cThe date, band, and exposure time (in minutes) of the AO observations.

^dThe PSF star used in analyzing each galaxy image.

^eThe FWHM (in arcseconds) and Strehl ratio (in percentage) for each PSF star. Two values are given for those PSF stars for which there were two images at a given wavelength during the same observing run.

Table 2. Derived Parameters

Name	Disk		Bulge		Redshift
	r_e^a	μ_o^b	r_e^a	μ_o^b	
PPM91714+22-19	$0.81^{+0.46}_{-0.19}$	$19.0^{+0.8}_{-0.6}$	$0.119^{+0.022}_{-0.022}$	$15.2^{+0.5}_{-0.5}$	0.46
PPM102164+18-1	$0.29^{+0.09}_{-0.07}$	$17.5^{+0.4}_{-0.3}$	$0.053^{+0.013}_{-0.017}$	$15.0^{+0.5}_{-0.5}$	0.55
PPM114182+6+27	$0.43^{+0.07}_{-0.08}$	$18.1^{+0.1}_{-0.2}$	$0.045^{+0.011}_{-0.009}$	$15.4^{+0.5}_{-0.4}$	0.48 ± 0.05^c
PPM91088-21+18	$0.49^{+0.07}_{-0.13}$	$18.6^{+0.1}_{-0.4}$	$0.084^{+0.015}_{-0.015}$	$16.6^{+0.5}_{-0.5}$	0.70
PPM101029+20-8	$0.24^{+0.10}_{-0.08}$	$18.0^{+0.3}_{-0.2}$	$0.025^{+0.017}_{-0.009}$	$16.0^{+0.7}_{-0.5}$	0.6 ± 0.3^d
PPM50296-7-23	$0.38^{+0.11}_{-0.15}$	$18.0^{+0.2}_{-0.8}$	$0.028^{+0.006}_{-0.015}$	$14.8^{+0.5}_{-0.4}$	0.6 ± 0.3^d
PPM91714+18-17	$0.55^{+0.18}_{-0.32}$	$20.6^{+0.2}_{-2.6}$	$0.130^{+0.042}_{-0.054}$	$16.8^{+0.7}_{-0.6}$	0.46
PPM106365-23+18	$0.48^{+0.62}_{-0.12}$	$19.2^{+1.4}_{-0.4}$	$0.076^{+0.144}_{-0.036}$	$18.2^{+1.1}_{-0.8}$	0.60
PPM127095-8+16	$0.46^{+0.59}_{-0.19}$	$19.2^{+2.4}_{-0.8}$	$0.070^{+0.200}_{-0.042}$	$17.6^{+3.0}_{-0.9}$	0.6 ± 0.3^d
PPM106365+4+13	$0.27^{+0.49}_{-0.09}$	$19.5^{+2.0}_{-0.4}$	$0.089^{+0.090}_{-0.082}$	$20.0^{+2.3}_{-1.8}$	0.6 ± 0.3^d

^aExponential scale length of each component in arcsec.

^bCentral surface brightness of each component in magnitudes arcsec⁻².

^cBased only on a spectral break.

^dBased on the photometric limit of the sample.